Results in Geophysical Sciences 14 (2023) 100056

Contents lists available at ScienceDirect

Results in Geophysical Sciences

journal homepage: www.sciencedirect.com/journal/results-in-geophysical-sciences

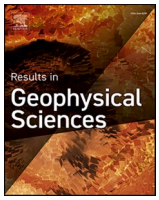

GNSS-based long-term deformation at Mount Etna volcano (Italy)

Mimmo Palano [a,b,*], Stefano Calcaterra [c], Piera Gambino [c], Benedetto Porfidia [c], Federica Sparacino [a]

[a] Istituto Nazionale di Geofisica e Vulcanologia, Sezione di Catania - Osservatorio Etneo, Catania, Italy
[b] Institute for Environmental Geology and Geoengineering (IGAG), National Research Council, Rome, Italy
[c] Italian Institute for Environmental Protection and Research (ISPRA), Rome, Italy

A B S T R A C T

We estimated a long-term velocity field for Mount Etna volcano by taking into account a dense GNSS dataset collected during the 2004.42 - 2018.95 period. To properly isolate the volcanic deformation from the background tectonic one, we defined a new local reference frame (termed MERF23) by using 32 stations mainly located in north-western and south-eastern Sicily. The computed long-term velocity field well highlights contrasting patterns between the north-western flank and the eastern one. The north-western flank was characterized by a general radial pattern with small deformations, mainly related to inflation and deflation episodes occurred during the investigated period. The eastern flank was characterized by a vigorous seaward motion, with rates ranging from ~60 mm/yr on the Pernicana fault (northern boundary) to ~29 mm/yr along the Aci Trezza fault (southern boundary), clearly evidencing as flank instability remains by far the predominant type of deformation at Mount Etna. A small contraction along the peripheral base of the volcano, coupled with a small uplift has been also detected; both patterns lend credit to the concurrent action of different processes as local and regional tectonics as well as long-term magmatic doming.

1. Introduction

The monitoring of ground surface deformation on active volcanoes over a long period of time helps improve understanding of the volcano dynamics as well as assessing potential volcanic hazard. Mount Etna (Fig. 1; eastern Sicily, Italy) is one of the most monitored volcanoes in the world due to both its proximity to highly-urbanized areas and its almost continuous eruptive activity from its summit craters and fairly frequent lava flow eruptions from fissures opened on its flanks. The GNSS-based monitoring at Mount Etna volcano started in the summer of 1988, making this volcano one of those with the longest records of GNSS observations (Bonforte et al., 2016). This initial network was progressively improved over the time by different groups and agencies and nowadays the deformation of most sectors of the volcano edifice is measured by more than 220 survey-type benchmarks (Bonforte et al., 2016; Murray et al., 2018; De Guidi et al., 2018) and 47 continuous GNSS stations (Bruno et al., 2012; Palano et al., 2022). Results coming from these datasets have greatly improved the knowledge of i) the plumbing system of the volcano, highlighting its multi-layered nature with different levels of magma accumulation (e.g., Aloisi et al., 2011; Bruno et al., 2012; Palano et al., 2017) and ii) the steady-state seaward motion of the Mount Etna eastern flank as well as the occurrence of aseismic slow slip events (Palano, 2016; Palano et al., 2022).

The objective of this study is to analyze and describe the long-term ground deformation pattern at Mount Etna, taking advantage of the large GNSS dataset collected in the last two decades. Moreover, as the number of GNSS stations around Mount Etna has increased, as well as improvements in processing software, we also provided an updated definition of the local reference frame in order to properly isolate the local volcanic deformation from the regional tectonic pattern.

This paper provides new insights on the ground displacement behavior at Mount Etna volcano and may also help for hazard assessment of potential flank destabilizations at other basaltic volcanoes.

2. Background setting

Mount Etna is a composite basaltic volcano located on the hangingwall of the Apennine-Maghrebian accretionary wedge at the convergent margin between Eurasia and Africa plates (Fig. 1) on eastern Sicily (Southern Italy; Gvirtzman and Nur, 1999). The western and northern slopes of Mount Etna lie over a sedimentary basement formed by Miocene turbiditic deposits of the Apenninic-Maghrebian chain, while the southern and eastern slopes over early-middle Pleistocene foredeep marly-clays (accumulated along the Gela-Catania Foredeep at the front of the Apenninic-Maghrebian chain; Branca and Ferrara, 2013).

Volcanic activity started about 500 ka ago as inferred by the shallow sub-volcanic bodies (pillow lavas and hyaloclastic breccias) intercalated

* Corresponding author.
E-mail address: mimmo.palano@ingv.it (M. Palano).

https://doi.org/10.1016/j.ringps.2023.100056
Received 13 January 2023; Received in revised form 11 April 2023; Accepted 4 May 2023
Available online 9 May 2023

at the top of the foredeep sediments (Di Stefano and Branca, 2002). This early stage was characterized by discontinuous and scattered submarine eruptive activity which progressively renewed through fissure-type eruptions in a subaerial environment in response to a regional uplift of north-eastern Sicily (Di Stefano and Branca, 2002). In particular, fissure-type eruptions took place in a wide area corresponding to the present-day lower western and south-eastern flanks of the volcano edifice since 330 ka and 220 ka, respectively, leading to the formation of a primitive shield-volcano structure (Branca et al., 2008). Since 129 ka ago, the major eruptive centres progressively migrated towards the present-day Valle del Bove (Nicolosi et al., 2016), where a central-type volcanism, leading to the formation of the earlier stratovolcano structure, developed between 110 ka and 60 ka (De Beni et al., 2011). About 60 ka ago, volcanic activity shifted toward the present-day eruptive centres and was characterized by the emplacement of wide lava flow fields, gradually expanding on the sedimentary basement (Branca et al., 2008). The occurrence of several Plinian eruptions between 15 and 15.5 ka ago formed a wide summit caldera (Coltelli et al., 2000) over which a thick succession of superposed lava flows and pyroclastic successions piled up in the last 15 ka. Around 10 ka ago, the wide depression of the Valle del Bove formed in response to a large gravitational slope failure of the eastern flank of the volcano (Calvari et al., 2004). In the last 10 ka, the occurrence of both effusive and largely explosive volcanic activity, ranging from frequent activity at the summit craters and episodic flank eruptions along radial fissures, led to the formation of three main rift zones, to the west (W), south (S), and to the northeast (NE) (Fig. 1; Garduno et al., 1997).

Activity in historical time has been documented from Greek and Roman civilizations, as citations inside literature and, often linked to legends or relevant historical events, so that the correspondence between historical and geological data for most ancient eruptions (with the exception of few eruptions whose activity was particularly noteworthy, as for instance the 122 BCE Plinian eruption), is poorly constrained (Coltelli et al., 1998). The descriptions of volcanic activity became more continuous and systematic in the 17th century as a consequence of the large 1669 eruption which destroyed many villages on the southeast slope of Mount Etna and reached the western sector of the town of Catania on the Ionian coast (Branca and Del Carlo, 2004). Since then, a continuous production of documents and reports, coupled with an increasing quality and completeness of information, has provided a high detail of the quasi-persistent activity of Mount Etna. In particular, volcanic activity at Mount Etna showed a quite uniform rate of occurrence of flank eruptions during the 1600 - 1970 period, while a short-term increase of occurrence of eruptions has been observed after the 1971 eruption (Branca and Del Carlo, 2004).

The present-day Mount Etna has a central conduit, with five summit craters located immediately westward of the Valle del Bove depression (Fig. 1). The Voragine Crater (VC) is the oldest one, being represented in the iconography since the fourteenth century. The other craters formed in the last 110 years: the North-East Crater (NEC) in 1911, the Bocca Nuova Crater (BNC) in 1968, the South-East Crater (SEC) in 1971 and the New South-East Crater (NSEC) in 2006.

The inhomogeneous long-term updoming (De Guidi et al., 2014) coupled with the different geomechanical properties of the basement, have favoured the development of a 17 km-wide horseshoe-shaped depression beneath the eastern flank of the volcano (Branca and Ferrara, 2013). This complex basement topography gently dips in SE direction and would lead to the large-scale seaward motion of the eastern flank of Mount Etna as documented since the early 1980s (see Palano, 2016 and reference therein). Conversely, the volcano is buttressed to the north and west by the Apenninic-Maghrebian chain which prevents any spreading occurring in these directions. At the surface, the unstable sector is defined by a 25 km-wide horseshoe-shaped region (Fig. 1) which, encompassing the sedimentary depression, is delimited by the

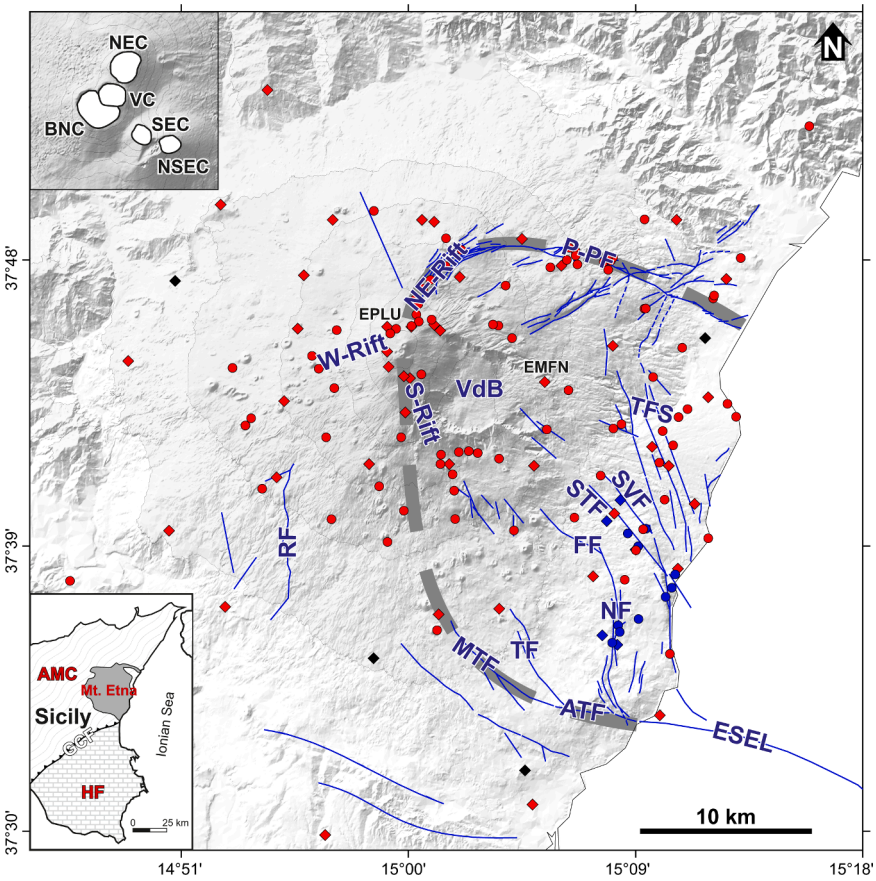

Fig. 1. Simplified tectonic map of Mount Etna and its eastern off-shore. The shaded gray line marks the unstable flank boundary. Continuous GNSS stations are reported as colored diamonds (red for INGV stations; blue for ISPRA stations; black for NetGEO and ItalPOS stations). Survey-type benchmarks are reported as colored points (red for INGV stations; blue for ISPRA stations). EMFN and EPLU are continuous GNSS stations. Other abbreviations are as follows: VdB, Valle del Bove; P-PF, Provenzana - Pernicana fault system; RF, Ragalna fault; TFS, Timpe fault system; SVF, Santa Venerina fault; STF, Santa Tecla fault; FF, Fiandaca fault; NF, Nizzeti fault system; TF, Trecastagni fault; MTF, Mascalucia-Tremestieri fault; ATF, Aci Trezza fault; ESEL, ESE lineament. The upper inset shows a zoom of the summit area of Mount Etna along with the active craters; NEC, North-East Crater; BNC, Bocca Nuova Crater; VC, Voragine Crater; SEC, South-East Crater; NSEC, New South-East Crater. The lower inset show a sketch map of eastern Sicily; AMC, Apennine-Maghrebian chain; HF, Hyblean Foreland; GCF, Gela-Catania Foredeep.

"North-East Rift (NER) - Provenzana - Pernicana fault system (P-PF)" to the NE and by the "South Rift (SR) - Mascalucia - Tremestieri - Aci Trezza fault system (MTF - ATF)", to the SE (Fig. 1). However, other authors identify the right-lateral Ragalna fault (RF) as the south-western boundary of the unstable sector (e.g. Borgia et al., 1992; Rust and Neri, 1996). Furthermore, active tectonics also occurs in the unstable sector along several shallow faults such as the Timpe (TFS), the Santa Tecla (STF), the Santa Venerina (SVF), the Fiandaca (FF) and the Nizzeti (NF) (Fig. 1; Azzaro et al., 2012).

3. GNSS networks and data processing

3.1. GNSS networks

As mentioned above, the use of GNSS for monitoring the ground deformation at Mount Etna volcano started in the summer of 1988 by the International Institute of Volcanology of Catania (now part of the Istituto Nazionale di Geofisica e Vulcanologia - INGV) with the establishment of a network of 18 survey-type benchmarks (Bonforte et al., 2016). The setting up of a continuous GNSS network began in November 2000 reaching a configuration of 13 stations in late summer of 2001 (Palano et al., 2010). Both networks were gradually upgraded over the years in order to cover all the slopes of the volcano and to replace the sites destroyed by lava flows, vandalism and/or affected by local instability (Fig. 1).

In late 2005, the Geodetic Group of the Geological Survey of Italy - ISPRA established a network of 5 continuous GNSS stations and 10 survey-type benchmarks across some faults in the south-eastern slope of the volcano (Fig. 1). Other 4 continuous GNSS stations have been established on the eastern (NetGEO, http://www.netgeo.it/) and the western and southern (ItalPOS, https://hxgnsmartnet.com/it-it) flanks of the volcano since 2012 and were discontinuously operating until the time of this writing (Fig. 1).

Other survey-style networks have been developed over the time at Mount Etna by different research groups (Murray et al., 2018; De Guidi et al., 2018). In the following, we analyzed the dataset collected by the networks mentioned above, while a dense geodetic solution including all the available GNSS datasets would be an interesting target for a future study.

3.2. GNSS data processing

All collected raw GNSS observations, spanning the 1995.0 - 2019.5 period, were processed by using the GAMIT/GLOBK software (Herring et al., 2018) and by taking into account precise ephemerides and Earth orientation parameters from the IGS (International GNSS Service; https://cddis.nasa.gov/archive/gnss/products) and from the International Earth Rotation Service (http://www.iers.org), respectively. To improve the overall configuration of the network and to provide an updated definition of the local reference frame, we introduced into the processing more than 160 continuous GNSS stations mostly located in southern Italy (Fig. 2a). During the processing, in order to eliminate the phase biases related to drifts in the satellite and receiver clock oscillators, an ionosphere-free linear combination of GNSS phase observables was adopted by applying a double differencing technique. The GNSS phase data were weighted according to an elevation-angle-dependent error model, while the IGS absolute antenna phase center models for both satellite and ground-based antennas were adopted. The first-order

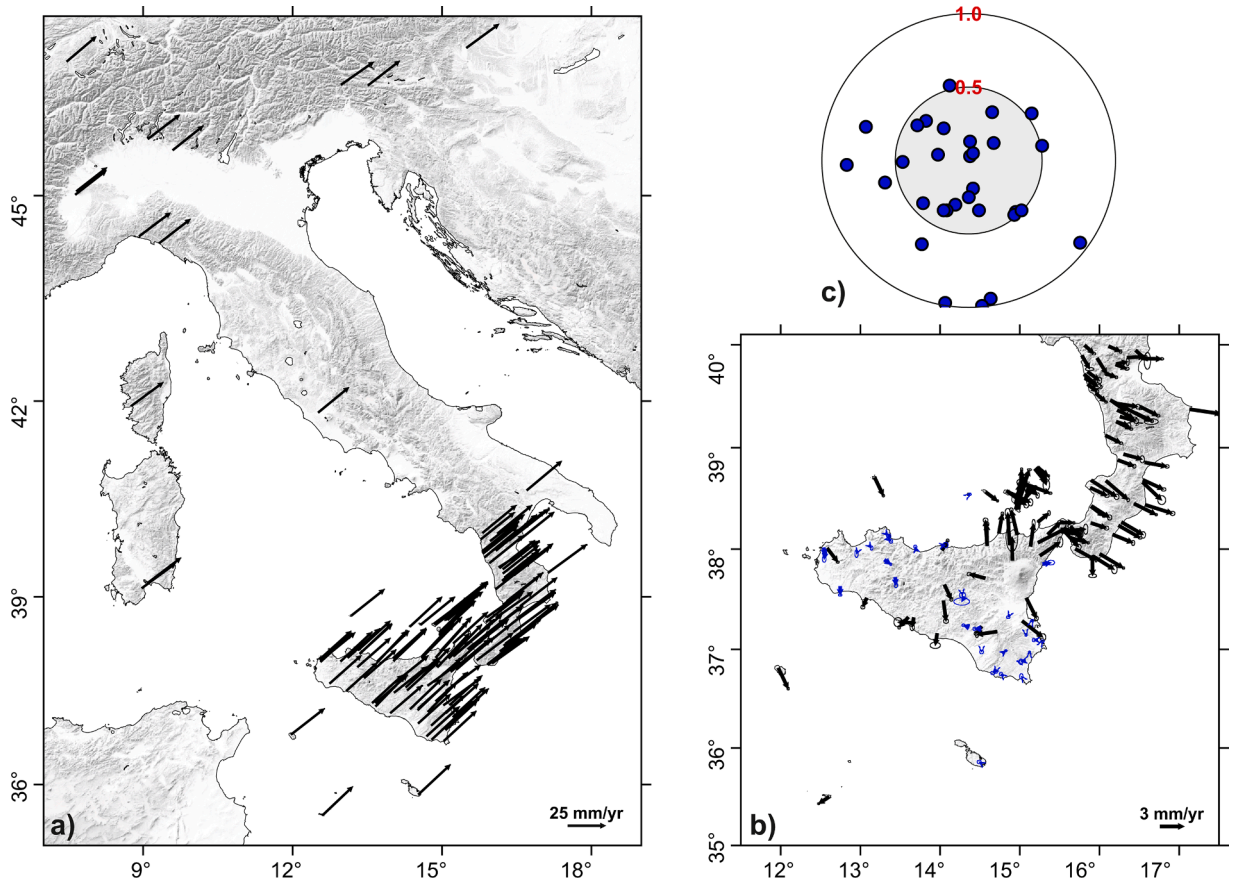

Fig. 2. a) ITRF14 velocities computed in this study. b) Residual velocity with respect to the MERF23 frame. Blue vectors represent the 32 GNSS stations used to the final Euler vector components estimation (Table 1). c) East and North component of the residuals (in mm/yr) of the 32 GNSS stations allowing the final estimation. See text in Section 3 for more details.

ionospheric delay was eliminated by using the ionosphere-free linear combination, while the IONEX files from the Crustal Dynamics Data Information System (https://cddis.nasa.gov/archive/gnss/products/ionex/) were used to apply a second-order ionospheric corrections (Petrie et al., 2010). The tropospheric delay was modeled as a piecewise linear model and estimated by adopting the VMF1 grids (Boehm et al., 2006). The Earth Orientation Parameters were tightly constrained to their a-priori values according to the IERS Bulletin B (https://maia.usno.navy.mil/products/iers-bulletins), while the FES2004 model (Lyard et al., 2006) was adopted for the ocean tidal loading. As results of the GAMIT step processing, daily estimates of loosely constrained station coordinates along with the associated variance-covariance matrices have been obtained. The daily GAMIT solutions were combined into GLOBK to estimate stations daily coordinates in the ITRF14 reference frame (Altamimi et al., 2016) as a first step, and the long-term ITRF14 velocities for a subset of stations not including the ones covering the volcano edifice, in a final step. Such a long-term ITRF14 solution was used as input for the Euler vector components estimation of the local reference frame, as described below.

3.3. The Mount Etna reference frame (MERF23)

Palano et al. (2010) computed a local reference frame to i) isolate the Mount Etna volcanic deformation from the background tectonic pattern and ii) allow a direct combination and comparison between different deformation episodes (inflation, deflation, dike intrusion) affecting the volcano edifice over the time. As the number of GNSS stations around the volcano and positioning precision have strongly increased, as well as improvements in underlying models and refinements in processing software, here we performed an updated definition of the local reference frame also. To this aim, we estimated the angular velocity of the local reference frame by minimizing, with a weighted least squares inversion, the adjustments to horizontal ITRF14 velocities of the stations located within a ~350-km radius around the volcanic edifice (Fig. 2a). In order to objectively determine the set of GNSS stations around the volcano that best defines a rigid block, we performed several tests by comparing the results from different estimations to detect which model best fits the data, considering a F-ratio criterion (Cannavò and Palano, 2016). Hence, we performed more than 30 tests, excluding each time all stations not satisfying the F-ratio criterion. Finally, a total of 32 stations passed the F-ratio criterion (Fig. 2b) allowing the Euler vector components estimation as reported in Table 1. Most of the residual values are lower than 1 mm/yr (Fig. 2c) and standard deviations for East and North components of the 32 stations are 0.29 mm/yr and 0.28 mm/yr, respectively, therefore highlighting as i) the block rigidity assumption has been respected and ii) the Euler pole estimation has been highly accurate. Moreover, the 32 stations used for the pole definition are mainly located in north-western and south-eastern Sicily, while stations located in north-eastern Sicily and Calabria show residuals larger than 3 mm/yr (Fig. 2b). Such a feature well reflects the current active tectonics of the area where i) north-eastern Sicily and Calabria are moving in response to the subduction process beneath the Calabrian Arc (Palano et al., 2017) and ii) most of the Eurasia-Africa convergence is currently adsorbed in the offshore of northern Sicily (Billi et al., 2023).

3.4. GNSS time-series and long-term velocity estimations

In the following, the estimated time-series as well as the long-term GNSS velocity field have been referred to the updated reference frame (hereinafter MERF23). By considering the East component time-series (Fig. 3) of two of the oldest GNSS stations at Mount Etna, as EPLU (located closely to the summit area) and EMFN (located on the eastern flank), at least 5 significant jumps related to shallow intrusion episodes (feeding volcanic activity) can be easily observed. All these jumps are clearly visible on the EPLU time-series, while only the jumps related to the intrusions that occurred in 2001, 2002 and 2018 are visible on the EMFN time-series. Such a different feature is related to the magnitude of the intrusive episodes: large intrusions (as the 2001, 2002 and 2018 ones) generate volcano-scale deformations, while small intrusions (as the ones occurred in 2008 and 2014) generate a pattern of deformation strictly confined to the summit portion of the volcano. Furthermore, the EMFN time-series is characterized by a time-dependent deformation following the 2002 intrusion, while exhibits a linear pattern at least during the 2004.40 - 2018.95 period. Based on these observations, we estimated a long-term GNSS velocity field for Mount Etna volcano (Fig. 4) by taking into account all GNSS observations collected during the 2004.42 - 2018.95 period, excluding all stations located around the summit area, above an altitude of 3000 m.

Table 1
Euler pole parameters for the Mount Etna Reference Frame (hereinafter, MERF23).

	Latitude (deg)v	Longitude (deg)	Rotation (deg/My)
MERF23	46.788 ± 1.883	−93.675 ± 3.493	0.271,347 ± 0.003993

3.5. Horizontal strain-rate computation

To provide additional insights into the present deformation pattern of the study area, we also estimated the horizontal strain-rate field according to Shen et al. (2015). We interpolated the velocity gradients on regularly 0.02° x 0.02° spaced grid from the observed GNSS velocities by least squares inversion. The method considers optimal weighting functions of the data, allowing analysts to obtain a finer resolution, especially on regions characterized by sparsely distributed data. The weight for each observation is given by the product of the area of the Voronoi cell occupied by the GNSS site and a Gaussian weight $(\exp(-\Delta R_{ij}^2/D_j^2))$, where *Rij* is the distance of site *i* from the grid point *j* and *Dj* is a smoothing parameter determined for each evaluation site based on the "in situ data strength", so that the total weight of observations on each grid point is the same. The estimated strain-rate field is reported in Fig. 5.

4. Results

The long-term GNSS velocity field for Mount Etna volcano (Fig. 4) spans the overall 2004.42 - 2018.95 period and was estimated with datasets covering different time intervals. The continuous GNSS stations managed by ISPRA discontinuously worked from mid-2005 to mid-2016, while the ones managed by ItalPOS and NetGEO discontinuously worked since 2007.50 and 2012.12, respectively. With the exception of some few stations, the ones managed by INGV cover the entire considered time interval. Concerning the survey-type benchmarks, the data collected by ISPRA cover the 2005.71 - 2012.95 time interval, while the ones collected by INGV span the 2004.42 - 2013.46 period. Despite these different time spans, all estimated horizontal velocities show a high coherent pattern, in term of magnitude and orientation, therefore in the following we considered them as fully representative for the overall 2004.42 - 2018.95 period. Looking at the horizontal velocity field (Fig. 4a), the seaward motion of the eastern flank of the volcano represents the most impressive pattern. The highest values (up to ~60 mm/yr) are measured closely to the Pernicana fault, while values generally larger than 35 mm/yr (black arrows in Fig. 4a) concentrate in the northern half of the unstable sector, including also the coastal sector eastward the Timpe fault system. Northward of the Pernicana fault, velocities range from ~5 mm/yr to ~2.5 mm/yr, on the western and eastern segments of the fault, respectively. The north-eastern edge of the unstable sector is characterized by an abrupt decrease of velocities, with values of ~18 mm/yr across the southernmost splay of the Pernicana fault. On the southern half of the unstable sector, a reduction of velocity can be easily recognized (Fig. 4a). In

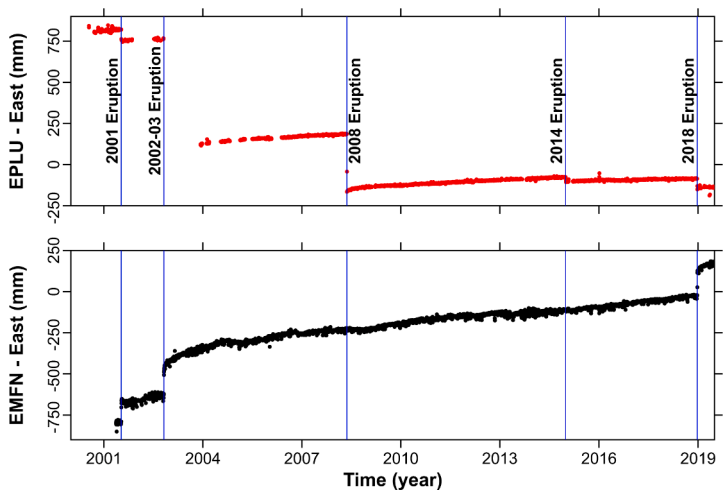

Fig. 3. Time-series of the East component of EPLU and EMFN stations. The vertical blue lines mark the shallow intrusions onset occurred in the analyzed time interval.

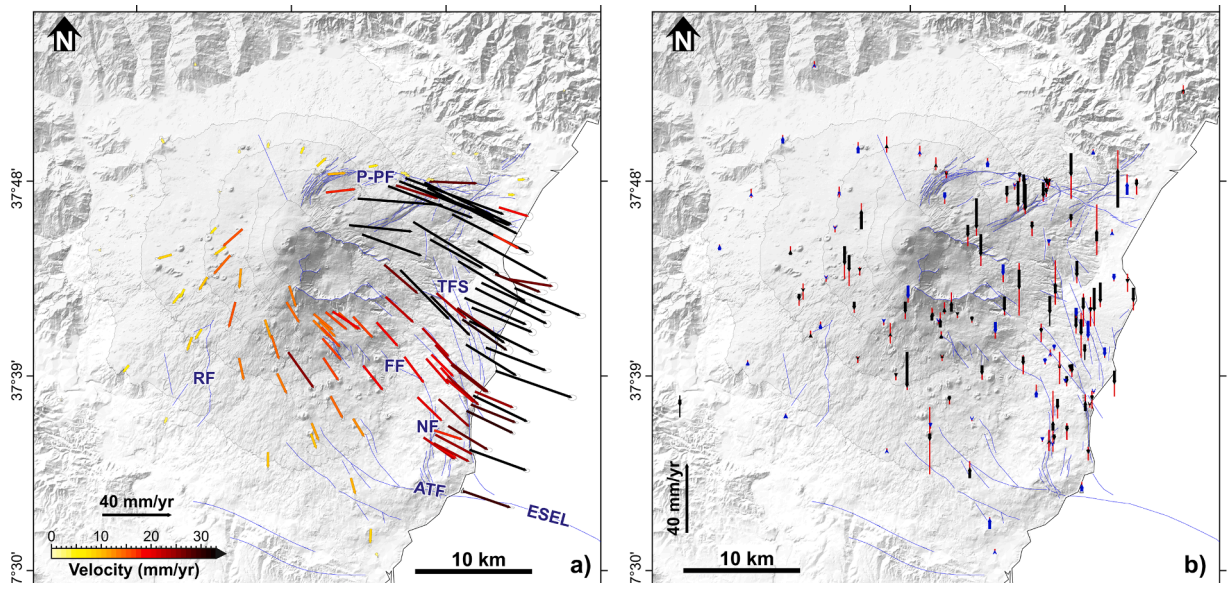

Fig. 4. Long-term (2004.42 - 2018.95) GNSS horizontal (panel a) and vertical (panel b) velocity field with 95% confidence ellipses for Mount Etna, in the MERF23 frame. Blue and black arrows on panel b stand for continuous stations and survey-type benchmarks, respectively. Abbreviations are as Fig. 1.

particular, the stations located eastward of the Timpe fault system have large velocity values (~40 mm/yr, on average) and move toward the ~N115°E direction, while those located westward have moderate velocity values (~15 mm/yr, on average) and move toward the ~N140°E direction. The south-western flank is characterized by a progressive south-eastward velocity decrease (from ~15 mm/yr close to the summit area, to ~4 mm/yr at the base of the volcano), while both the north-western and northern flanks show small deformations (lesser than 5 mm/yr, on average). The peripheral base of the volcano is also characterized by small velocities (Fig. 4a).

Regarding the vertical velocities, estimations at survey-type benchmarks are slight larger than the ones estimated at continuous GNSS stations, and generally characterized by large uncertainties. These features could be related to the limited number of measurements (ca. 2–3 measurements every year) collected at each survey-type benchmark, so that their vertical velocity estimation is less accurate. Keeping in mind this limitation, on the volcano edifice, the estimated height variations (Fig. 4b) are generally negative with the highest values along the southern rim of the Pernicana fault (~15 mm/yr) and across the Timpe fault system (~10 mm/yr). A very small uplift (1–3 mm/yr) can be observed at the continuous stations located along the peripheral base of the volcano.

The strain-rate field is dominated by high values along the Pernicana fault and the coastal belt on both the Nizzeti and the Timpe fault system (Fig. 5). In particular, along the Pernicana fault, the strain-rate field is characterized by values up to 12 μstrain/yr with NW-SE-oriented extensional axes, while the coupled contractional axes show values up to 8 μstrain/yr. Across the Nizzeti and the Timpe fault system, the strain axes are characterized by values up to 7 μstrain/yr and have a E-W prevalent orientation (Fig. 5). A similar pattern can be observed also on the summit area of the volcano. In all these sectors, the overall areal change pattern is positive (Fig. 5) evidencing their general extensional pattern. The north-eastern edge of the unstable sector is characterized by strain axes with a E-W orientation and a dominant contractional pattern. This pattern clearly highlights the main role of the southernmost splay of the Pernicana fault in transferring the overall seaward motion of the unstable flank (Palano et al., 2006). Moreover, such a long-term contractional pattern contrasts with the short-term extensional pattern

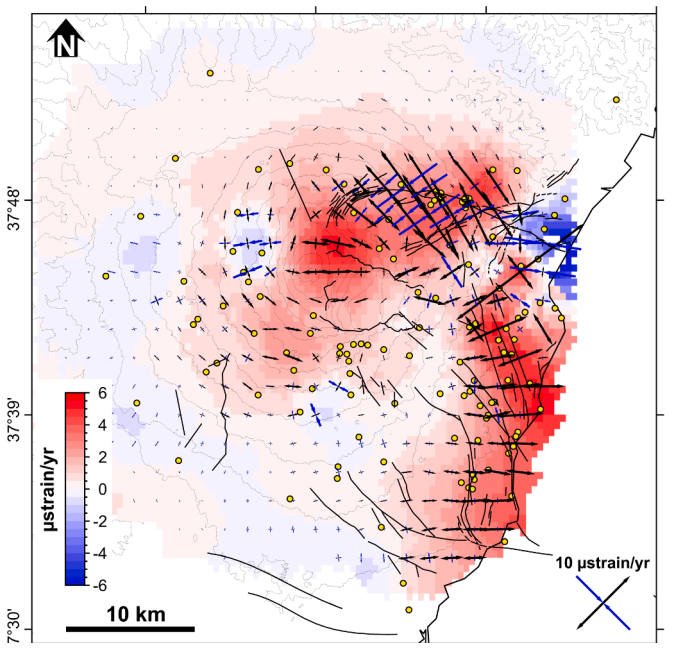

Fig. 5. Geodetic strain-rate field: background color reports the magnitude of the rate of areal change, while arrows represent the greatest extensional (black) and contractional (blue) horizontal strain-rates. The yellow circles represent the GNSS stations used for the computation.

related to the occurrence of slow slip events (Palano et al., 2022). A very small contractional pattern with radially oriented strain axes is also observed on the peripheral base of the volcanic edifice (Fig. 5).

5. Discussion

The dense long-term GNSS velocity field along with the related strain-rate pattern for Mount Etna volcano depict some interesting features. As above mentioned, the most impressive pattern is given by the seaward motion of the eastern flank with rates ranging from ~60 mm/yr on the Pernicana fault to ~29 mm/yr along the Aci Trezza fault. These values can be considered representative of the current slip-rates of the faults bordering the unstable sector (Fig. 1). Indeed, the value of 60 mm/yr is twice larger than the one estimated for the 1997–2001 period, highlighting a marked change in the slip-rate of the left-lateral Pernicana fault after the 2002–2003 eruption (Palano et al., 2009). The faults bordering the southern edge of the unstable sector account for a right lateral slip-rate of ~29 mm/yr, which is an order of magnitude higher than the ones estimated from geologic marker offsets (Azzaro et al., 2012). The different slip-rate observed along the faults bordering the unstable sector is not related to the sedimentary basement topography (Branca and Ferrara, 2013) but would be probably related to the presence of heterogeneities within the sedimentary basement. Moreover, the pattern of motion within the eastern flank is also controlled by the Nizzeti and the Timpe fault system. In particular, the stations located along the coastal belt have large velocity values (~40 mm/yr, on average) and move toward the ~N115°E direction, while those located westward of the Timpe fault system have moderate velocity values (~15 mm/yr, on average) and move toward the ~N140°E direction.

Another interesting pattern is the areal contraction and the small uplift (1–3 mm/yr) observed along the peripheral base of the volcanic edifice (Fig. 5). A similar pattern has been observed also on long-term InSAR velocity maps and interpreted as the continuous growth of a peripheral bulge due to load of the volcano along a weak basement (Solaro et al., 2010). Indeed, the uplift of peripheral base of Mount Etna has been documented by geological observations and it was related to different sources as the growth of a basal anticlines (Borgia et al., 1992), regional tectonics (Bousquet et al., 1988; Catalano et al., 2004) and long-term magmatic doming (De Guidi et al., 2014). Our data alone cannot discriminate among the different contribution, however our geodetic uplift rate is larger than the ones estimated geologically (0.3 - 0.5 mm/yr; Di Stefano and Branca, 2002; Catalano et al., 2004), therefore the concurrent action of all the mentioned processes cannot be ruled out.

Some new insights can be inferred by taking the instrumental seismicity into account (Fig. 6a). Shallow seismicity (depth < 10 km) is mainly located beneath the summit area, the upper portions of the southern and eastern flanks and along the western sector of the Provenzana - Pernicana fault system. Shallow seismicity beneath the north-western flank is scant and became abundant at depth larger than 20 km. By considering the A-A' cross-section (Fig. 6b), the depth distribution of seismicity beneath the north-western flank clearly depicts the bending of the Hyblean continental lithosphere beneath the thrust nappes of the Apenninic-Maghrebian chain (Chiarabba and Palano, 2017). At shallow depth, the abrupt transition between the elastic crust (north-western flank) and the fragile one (south-eastern flank), occurs beneath the summit area and marks also the location of all the inflation and deflation sources modelled in the last decades (Palano et al., 2008, 2017; Aloisi et al., 2011; Bruno et al., 2012; Gonzalez and Palano, 2014; Cannata et al., 2015; Spampinato et al., 2015; Viccaro et al., 2016; Gambino et al., 2016; Camacho et al., 2020, Fig. 6b).

Since the spatial pattern of the shallow seismicity shows some similarities with the geodetic one (Fig. 4a and Fig. 5), we performed a simple comparison between both (Fig. 6c). We therefore considered the strain-rate variation (in terms of areal dilatation) and the number of shallow (gray histogram; depth ≤ 10 km) and deep (red histogram; depth > 10 km) earthquakes along the A-A' cross-section. No significant correlations arise from the comparison of the geodetic areal dilatation and the number of deep earthquakes. Conversely, a good correlation between the geodetic areal dilatation and the number of shallow earthquakes (here considered as a gross measure of the seismic release, given the 1.2–4.9 range of recorded magnitude) can be observed for the $-20 \div 15$ km horizontal range of the A-A' cross-section. However, both patterns are poorly correlated for the south-easternmost portion of the analysed cross-section in correspondence of the Nizzeti and the Timpe fault system, where despite the occasional occurrence of moderate earthquakes (Azzaro et al., 2013), the large deformation is not balanced by the seismic release, remarking the prevalent aseismic behavior of these faults. Aseismic deformation is also associated to slow slip events nucleating along a shallow sliding surface, as well observed during the last decade (Palano et al., 2022).

Conclusive remarks

The long-term dense GNSS velocity field at Mount Etna well highlight the contrasting patterns between the small deformation of the north-western flank (buttressed by the presence of the Apenninic-Maghrebian chain) and the large deformation of the eastern flank (amplified by the lack of buttressing by surrounding material). Within the eastern flank, the deformation doesn't occur homogeneously and shows a set of different patterns along both the faults bordering/cutting the unstable sector, probably related to heterogeneities in the sedimentary basement. We observed also a small contraction along the peripheral base of the volcanic edifice, which coupled with a small uplift suggest the concurrent action of different processes as local and regional tectonics as well as long-term magmatic doming. A simple comparison between shallow seismicity and the geodetic strain-rate reveals a good correlation for the north-western flank, the summit area and the upper south-eastern flank; conversely, both patterns are poorly correlated for the lower south-eastern flank evidencing the prevalent aseismic behavior of active faults cutting it. These results may help also in constraining active deformation sources, therefore providing useful information on the magmatic plumbing system of Mount Etna volcano along

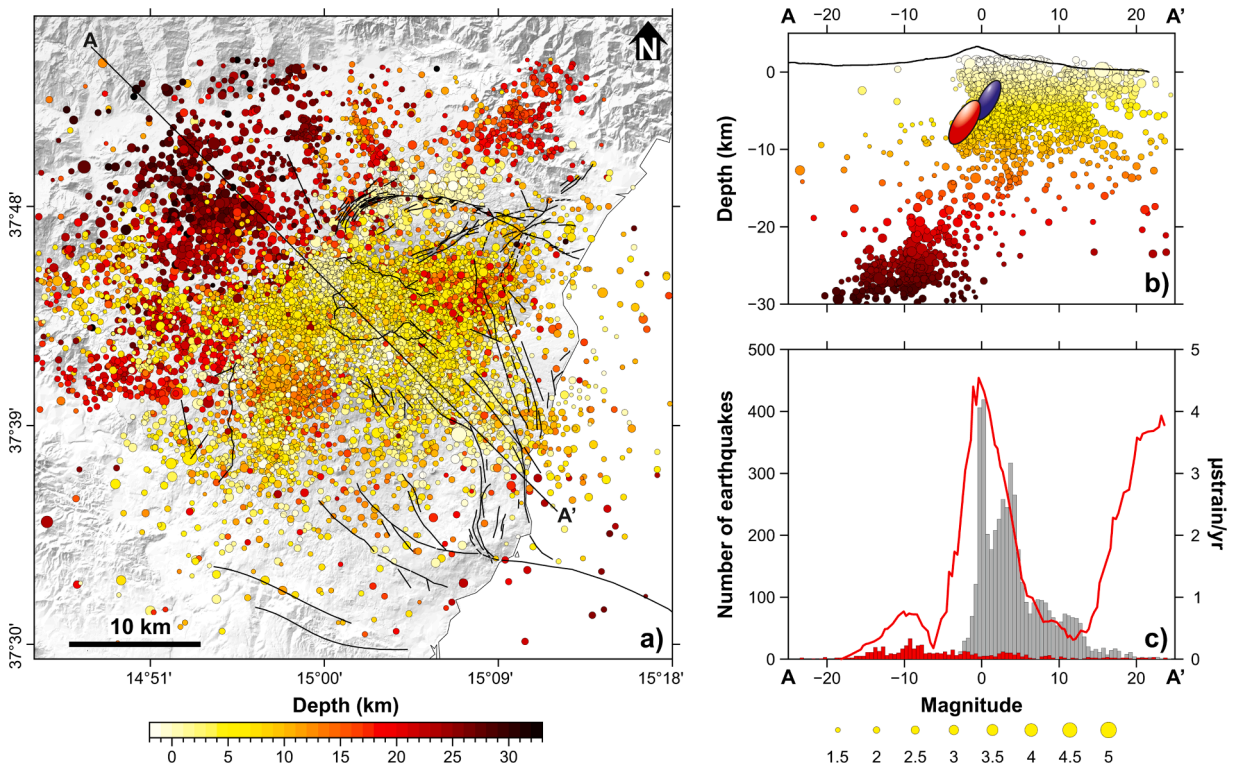

Fig. 6. a) Instrumental seismicity with magnitude larger than 1.2 occurred at Mount Etna volcano during the 2000 - 2019.5 time interval (Alparone et al., 2015, 2020a, 2020b, 2022). b) Instrumental seismicity with magnitude larger than 1.2 located within ±2.5 km from the profile trace A-A'. Red and blue ellipses represent the volumes in which most of the inflating and deflating sources modelled in the last two decades concentrate, respectively. c) Histograms (0.5 km bins) for seismicity with depth ≤ 10 km (gray histogram) and with depth > 10 km (red histogram). The red line stands for the areal change variations.

with its interaction with other processes such as flank instability, active faults, etc. Achieved results highlight how dense continuous and episodic geodetic networks may help revealing and understanding complex deformations at other basaltic volcanoes as Mount Etna and may also add useful constraints for the hazard assessment of potential flank destabilizations.

Web-sites

International GNSS Service. http://igscb.jpl.nasa.gov (accessed on 10 January 2023).

International Earth Rotation and Reference Systems Service. http://www.iers.org (accessed on 10 January 2023).

NetGEO RETE GNSS. http://www.netgeo.it (accessed on 09 January 2023).

Crustal Dynamics Data Information System (CDDIS). https://cddis.nasa.gov/archive/gnss/products/ionex/ (accessed on 09 January 2023).

HEXAGON SmartNet. https://hxgnsmartnet.com/it-it (accessed on 10 January 2023).

IERS Bulletins. https://maia.usno.navy.mil/products/iers-bulletins (accessed on 10 January 2023).

Declaration of Competing Interest

All the authors know and concur with the submission of this manuscript to **Results in Geophysical Sciences** journal and declare no conflict of interests.

Data availability

Data will be made available on request.

Acknowledgments

The GNSS data used in this study have been processed in the framework of the Project "Paroxysmal volcanic events and seaward motion at Mt. Etna: an improved picture from a geodetic and seismological perspective" (Progetti di Ricerca Libera) funded by INGV.

References

Aloisi, M., Mattia, M., Ferlito, C., Palano, M., Bruno, V., Cannavò, F., 2011. Imaging the multi-level magma reservoir at Mt. Etna volcano (Italy). Geophys. Res. Lett. 38 (16), L16306. https://doi.org/10.1029/2011gl048488.

Alparone, S., Maiolino, V., Mostaccio, A., Scaltrito, A., Ursino, A., Barberi, G., D'Amico, S., Di Grazia, G., Giampiccolo, E., Musumeci, C., Scarfì, L., Zuccarello, L., 2015. Mt. Etna seismic catalog 2000-2010 [Data set]. Istit. Nazion. Geofis. Vulcanol. (INGV) - Osservatorio Etneo. https://doi.org/10.13127/etnasc/2000_2010.

Alparone, S., Barberi, G., Di Grazia, G., Giampiccolo, E., Maiolino, V., Mostaccio, A., Musumeci, C., Scaltrito, A., Ursino, A., 2020a. Mt. Etna seismic catalog 2011-2013 (Version 1) [Data set]. Istit. Nazion. Geofis. Vulcanol. (INGV). https://doi.org/10.13127/ETNASC/2011_2013.

Alparone, S., Barberi, G., Di Grazia, G., Giampiccolo, E., Maiolino, V., Mostaccio, A., Musumeci, C., Scaltrito, A., Tuvè, T., Ursino, A., 2020b. Mt. Etna seismic catalog 2014-2016 (Version 1) [Data set]. Istit. Nazion. Geofis. Vulcanol. (INGV). https://doi.org/10.13127/ETNASC/2014_2016.

Alparone, S., Barberi, G., Di Grazia, G., Giampiccolo, E., Maiolino, V., Mostaccio, A., Musumeci, C., Scaltrito, A., Tuvè, T., Ursino, A., 2022. Mt. Etna seismic catalog 2017-2019 (Version 1) [Data set]. Istit. Nazion. Geofisica Vulcanol. (INGV). https://doi.org/10.13127/ETNASC/2017_2019.

Altamimi, Z., Rebischung, P., Métivier, L., Collilieux, X., 2016. ITRF2014: a new release of the International Terrestrial Reference Frame modeling nonlinear station motions. J. Geophys. Res. 121, 6109–6131. https://doi.org/10.1002/2016JB013098.

Azzaro, R., Branca, S., Gwinner, K., Coltelli, M., 2012. The volcano-tectonic map of Etna volcano, 1:100.000 scale: morphotectonic analysis from high-resolution DEM integrated with geologic, active faulting and seismotectonic data. It. J. Geosci. (Boll. Soc. Geol. It.) 131 (1), 153–170. https://doi.org/10.3301/IJG.2011.29.

Azzaro, R., D'Amico, S., Peruzza, L., Tuvè, T., 2013. Probabilistic seismic hazard at Mt. Etna (Italy): the contribution of local fault activity in mid-term assessment. J. Volcanol. Geotherm. Res. 251, 158–169. https://doi.org/10.1016/j.jvolgeores.2012.06.005.

Billi, A., Cuffaro, M., Orecchio, B., Palano, M., Presti, D., Totaro, C., 2023. Retracing the Africa–Eurasia nascent convergent boundary in the Western Mediterranean based on earthquake and GNSS data. Earth Planet. Sci. Lett. 601, 117906 https://doi.org/10.1016/j.epsl.2022.117906.

Boehm, J., Werl, B., Schuh, H., 2006. Troposphere mapping functions for GPS and very long baseline interferometry from European centre for medium range weather forecasts operational analysis data. J. Geophys. Res. 111, B02406. https://doi.org/10.1029/2005JB003629.

Bonforte, A., Fagone, S., Giardina, C., Genovese, S., Aiesi, G., Calvagna, F., Cantarero, M., Consoli, O., Consoli, S., Guglielmino, F., Puglisi, B., Puglisi, G., Saraceno, B., 2016. Global positioning system survey data for active seismic and volcanic areas of eastern Sicily, 1994 to 2013. Sci. data 3 (1), 1–13. https://doi.org/10.1038/sdata.2016.62.

Borgia, A., Ferrari, L., Pasquarè, G., 1992. Importance of gravitational spreading in the tectonic and volcanic evolution of Mount Etna. Nature 357 (6375), 231–235. https://doi.org/10.1038/357231a0.

Bousquet, J.C., Lanzafame, G., Paquin, C., 1988. Tectonic stresses and volcanism: in-situ stress measurements and neotectonic investigations in the Etna area (Italy). Tectonophysics 149 (3–4), 219–231. https://doi.org/10.1016/0040-1951(88)90174-6.

Branca, S., Del Carlo, P., 2004. Eruptions of Mt Etna during the past 3.200 years: a revised compilation integrating the historical and stratigraphic records. Mt. Etna: Volcano Lab.

Branca, S., Ferrara, V., 2013. The morphostructural setting of Mount Etna sedimentary basement (Italy): implications for the geometry and volume of the volcano and its flank instability. Tectonophysics 586, 46–64. https://doi.org/10.1016/j.tecto.2012.11.011.

Branca, S., Coltelli, M., De Beni, E., Wijbrans, J., 2008. Geological evolution of Mount Etna volcano (Italy) from earliest products until the first central volcanism (between 500 and 100 ka ago) inferred from geochronological and stratigraphic data. Int. J. Earth Sci. 97 (1), 135–152. https://doi.org/10.1007/s00531-006-0152-0.

Bruno, V., Mattia, M., Aloisi, M., Palano, M., Cannavò, F., Holt, W.E., 2012. Ground deformations and volcanic processes as imaged by CGPS data at Mt. Etna (Italy) between 2003 and 2008. J. Geophys. Res.: Solid Earth 117 (B7). https://doi.org/10.1029/2011JB009114.

Calvari, S., T.anner, L.H., Groppelli, G., Norini, G., 2004. Valle Del Bove, Eastern Flank of Etna Volcano: a Comprehensive Model for the Opening of the Depression and Implications for Future Hazards. Etna Volcano Laboratory. American Geophysical Union.

Camacho, A.G., Fernández, J., Samsonov, S.V., Tiampo, K.F., Palano, M., 2020. Multisource 3D modelling of elastic volcanic ground deformations. Earth Planet. Sci. Lett., 116445 https://doi.org/10.1016/j.epsl.2020.116445, 547C.

Cannata, A., Spedalieri, G., Behncke, B., Cannavò, F., Di Grazia, G., Gambino, S., Gresta, S., Gurrieri, S., Liuzzo, M., Palano, M., 2015. Pressurization and depressurization phases inside the plumbing system of Mount Etna volcano: evidence from a multiparametric approach. J. Geophys. Res.: Solid Earth 120 (9), 5965–5982. https://doi.org/10.1002/2015jb012227.

Cannavò, F., Palano, M., 2016. Defining Geodetic reference frame using Matlab®: platEMotion 2.0. Pure Appl. Geophys 173 (3), 937–944. https://doi.org/10.1007/s00024-015-1112-z.

Catalano, S., Torrisi, S., Ferlito, C., 2004. The relationship between late quaternary deformation and volcanism of Mt. Etna (eastern Sicily): new evidence from the sedimentary substratum in the Catania region. J. Volcanol. Geotherm. Res. 132 (4), 311–334. https://doi.org/10.1016/S0377-0273(03)00433-5.

Chiarabba, C., Palano, M., 2017. Progressive migration of slab break-off along the southern Tyrrhenian plate boundary: constraints for the present day kinematics. J. Geodyn. 105, 51–61. https://doi.org/10.1016/j.jog.2017.01.006.

Coltelli, M., Del Carlo, P., Vezzoli, L., 1998. Discovery of a Plinian basaltic eruption of Roman age at Etna volcano. Italy. Geol. 26 (12), 1095–1098. https://doi.org/10.1130/0091-7613(1998)026<1095:DOAPBE>2.3.CO;2.

Coltelli, M., Del Carlo, P., Vezzoli, L., 2000. Stratigraphic constraints for explosive activity in the past 100 ka at Etna Volcano, Italy. Int. J. Earth Sci. 89 (3), 665–677. https://doi.org/10.1007/s005310000117.

De Beni, E., Branca, S., Coltelli, M., Groppelli, G., Wijbrans, J.R., 2011. 40Ar/39Ar isotopic dating of Etna volcanic succession. Italian J. Geosci. 130 (3), 292–305. https://doi.org/10.3301/IJG.2011.14.

De Guidi, G., Imposa, S., Scudero, S., Palano, M., 2014. New evidence for late quaternary deformation of the substratum of Mt. Etna volcano (Sicily, Italy): clues indicate active crustal doming. Bull. Volcanol 76 (816). https://doi.org/10.1007/s00445-014-0816-8.

De Guidi, G., Brighenti, F., Carnemolla, F., Imposa, S., Marchese, S.A., Palano, M., Scudero, S., Vecchio, A., 2018. The unstable eastern flank of Mt. Etna volcano (Italy): first results of a GNSS-based network at its southeastern edge. J. Volcanol. Geotherm. Res. 357, 418–424. https://doi.org/10.1016/j.jvolgeores.2018.04.027.

Di Stefano, A., Branca, S., 2002. Long-term uplift rate of the Etna volcano basement (southern Italy) based on biochronological data from Pleistocene sediments. Terra Nova 14 (1), 61–68. https://doi.org/10.1046/j.1365-3121.2002.00389.x.

Gambino, S., Cannata, A., Cannavò, F., La Spina, A., Palano, M., Sciotto, M., Spampinato, L., Barberi, G., 2016. The unusual 28 December 2014 dike-fed paroxysm at Mount Etna: timing and mechanism from a multidisciplinary perspective. J. Geophys. Res.: Solid Earth 121 (3), 2037–2053. https://doi.org/10.1002/2015JB012379.

Garduño, V.H., Neri, M., Pasquarè, G., Borgia, A., Tibaldi, A., 1997. Geology of the NE Rift of Mount Etna, Sicily (Italy). Acta Vulcanol 9, 91–100.

González, P.J., Palano, M., 2014. Etna 2001 eruption: new insights into the magmatic system feeding and the mechanical response of the western flank from geodetic data. J. Volcanol. Geotherm. Res. 274, 108–121. https://doi.org/10.1016/j.jvolgeores.2014.02.001.

Gvirtzman, Z., Nur, A., 1999. The formation of Mount Etna as the consequence of slab rollback. Nature 401, 782–785. https://doi.org/10.1038/44555.

Herring, T.A., King, R., Floyd, M.A., McClusky, S.C., 2018. Introduction to GAMIT/GLOBK, Release 10.7. Massachusetts Institute of Technology, Cambridge, UK. https://www-gpsg.mit.edu.

Lyard, F., Lefevre, F., Letellier, T., Francis, O., 2006 Modelling the global ocean tides: modern insights from fes2004. Ocean Dyn. 56, 394–415. https://doi.org/10.1007/s10236-006-0086-x.

Murray, J.B., van Wyk de Vries, B., Pitty, A., Sargent, P., Wooller, L., 2018. Gravitational sliding of the Mt. Etna massif along a sloping basement. Bulletin Volcanol 80 (4), 1–11. https://doi.org/10.1007/s00445-018-1209-1.

Nicolosi, I., D'Ajello Caracciolo, F., Branca, S., Ferlito, C., Chiappini, M., 2016. The earliest open conduit eruptive center of the Etnean region: evidence from aeromagnetic, geophysical, and geological data. Bull. Volcanol. 78 (7), 1–11. https://doi.org/10.1007/s00445-016-1042-3.

Palano, M., Aloisi, M., Amore, M., Bonforte, A., Calvagna, F., Cantarero, M., Consoli, O., Guglielmino, F., Mattia, M., Puglisi, B., Puglisi, G., 2006. Kinematics and strain analyses of the eastern segment of the Pernicana fault (Mt. Etna, Italy) derived from geodetic techniques (1997 - 2005). Ann. Geophys 49, 1105–1117.

Palano, M., Puglisi, G., Gresta, S., 2008. Ground deformation patterns at Mt. Etna from 1993 to 2000 from joint use of InSAR and GPS techniques. J. Volcanol. Geotherm. Res. 169 (3–4), 99–120. https://doi.org/10.1016/j.jvolgeores.2007.08.014.

Palano, M., Gresta, S., Puglisi, G., 2009. Time-dependent deformation of the eastern flank of Mt. Etna: after-slip or viscoelastic relaxation? Tectonophysics 473, 300–311. https://doi.org/10.1016/j.tecto.2009.02.047.

Palano, M., Rossi, M., Cannavò, F., Bruno, V., Aloisi, M., Pellegrino, D., Pulvirenti, M., Siligato, G., Mattia, M., 2010. Etn@ref: a geodetic reference frame for Mt. Etna GPS networks. Ann. Geophys. 53 (4), 49–57. https://doi.org/10.4401/ag-4879.

Palano, M., 2016. Episodic slow slip events and seaward flank motion at Mt. Etna volcano (Italy). J. Volcanol. Geotherm. Res. 324, 8–14. https://doi.org/10.1016/j.jvolgeores.2016.05.010.

Palano, M., Viccaro, M., Zuccarello, F., Gresta, S., 2017. Magma transport and storage at Mt. Etna (Italy): a review of geodetic and petrological data for the 2002-03, 2004 and 2006 eruptions. J. Volcanol. Geotherm. Res. 347, 149–164. https://doi.org/10.1016/j.jvolgeores.2017.09.009.

Palano, M., Sparacino, F., Gambino, P., D'Agostino, N., Calcaterra, S., 2022. Slow slip events and flank instability at Mt. Etna volcano (Italy). Tectonophysics, 229414. https://doi.org/10.1016/j.tecto.2022.229414.

Petrie, E.J., King, M.A., Moore, P., Lavallée, D.A., 2010. Higher-order ionospheric effects on the GPS reference frame and velocities. J. Geophys. Res. 115 (B3), B03417. https://doi.org/10.1029/2009JB006677.

Rust, D., Neri, M., 1996. The Boundaries of Large-Scale Collapse on the Flanks of Mount Etna, Sicily, 110. Geological Society, London, pp. 193–208. https://doi.org/10.1144/GSL.SP.1996.110.01.15. Special Publications.

Shen, Z.K., Wang, M., Zeng, Y., Wang, F., 2015. Optimal interpolation of spatially discretized geodetic data. Bull. Seismol. Soc. Am. 105 (4), 2117–2127. https://doi.org/10.1785/0120140247.

Solaro, G., Acocella, V., Pepe, S., Ruch, J., Neri, M., Sansosti, E., 2010. Anatomy of an unstable volcano from InSAR: multiple processes affecting flank instability at Mt. Etna, 1994-2008. J. Geophys. Res. 115, B10405. https://doi.org/10.1029/2009JB000820.

Spampinato, L., Sciotto, M., Cannata, A., Cannavò, F., La Spina, A., Palano, M., Salerno, G.G., Privitera, E., Caltabiano, T., 2015. Multiparametric study of the February-April 2013 paroxysmal phase of Mt. Etna New South-East crater. Geochem. Geophys. Geosyst. 16 (6), 1932–1949. https://doi.org/10.1002/2015GC005795.

Viccaro, M., Zuccarello, F., Cannata, A., Palano, M., Gresta, S., 2016. How a complex basaltic volcanic system works: constraints from integrating seismic, geodetic, and petrological data at Mount Etna volcano during the July-August 2014 eruption. J. Geophys. Res.: Solid Earth 121 (8), 5659–5678. https://doi.org/10.1002/2016JB013164.